ACS SENSORS

pubs.acs.org/acssensors

Article

Multifunctional Nanoparticle Platform for Surface Accumulative Nucleic Acid Amplification and Rapid Electrochemical Detection: An Application to Pathogenic Coronavirus

Jeong Ook Soh,[⊥] Bum Chul Park,[⊥] Hyeon Su Park,[⊥] Myeong Soo Kim, Hong En Fu, Young Keun Kim,* and Ju Hun Lee*

Cite This: *ACS Sens.* 2023, 8, 839−847

Read Online

ACCESS | Metrics & More | Article Recommendations | Supporting Information

ABSTRACT: Of various molecular diagnostic assays, the real-time reverse transcription polymerase chain reaction is considered the gold standard for infection diagnosis, despite critical drawbacks that limit rapid detection and accessibility. To confront these issues, several nanoparticle-based molecular detection methods have been developed to a great extent, but still possess several challenges. In this study, a novel nucleic acid amplification method termed nanoparticle-based surface localized amplification (nSLAM) is paired with electrochemical detection (ECD) to develop a nucleic acid biosensor platform that overcomes these limitations. The system uses primer-functionalized Fe_3O_4−Au core−shell nanoparticles for nucleic acid amplification, which promotes the production of amplicons that accumulate on the nanoparticle surfaces, inducing significantly amplified currents during ECD that identify the presence of target genetic material. The platform, applying to the COVID-19 model, demonstrates an exceptional sensitivity of ∼1 copy/μL for 35 cycles of amplification, enabling the reduction of amplification cycles to 4 cycles (∼7 min runtime) using 1 fM complementary DNA. The nSLAM acts as an accelerator that actively promotes and participates in the nucleic acid amplification process through direct polymerization and binding of amplicons on the nanoparticle surfaces. This ultrasensitive fast-response system is a promising method for detecting emerging pathogens like the coronavirus and can be extended to detect a wider variety of biomolecules.

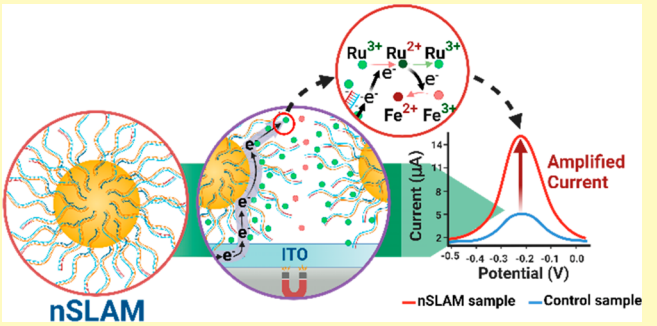

KEYWORDS: *DNA-functionalized nanoparticles, magnetic responsibility, gene amplification, electrochemical assay, nucleic acid biosensor, coronavirus, molecular diagnosis*

Over the past few years, the development of nucleic acid biosensors using nanomaterial-based electrochemical assays has gained much attention due to their rapid response, low cost, and exceptional sensitivity.[1] Efforts have been made to improve the sensitivity and selectivity of these biosensors by tuning the morphology (nanoparticles, nanotubes, nanochannels, etc.) and elemental components constituting the nanomaterials.[2] Nanoparticles (NPs) are a popular choice for research because of their electrochemical catalysis, surface conductivity, general accessibility, large surface area, excellent biocompatibility, and well-established bioconjugation chemistry with some functional groups.[3,4] Since the report of the first programmable assembly of DNA-functionalized NPs, research on their assembly has progressed to a great extent.[5,6] Considerable development of the nanostructure has taken place, particularly regarding electrochemical detection (ECD) of genetic material.[7,8] Thus, the significance of NPs as a nucleic acid biosensor platform for ECD is well recognized, and research in this field continues to produce notable results.

Since December 2019, COVID-19 (SARS-CoV-2, severe acute respiratory syndrome coronavirus 2), has caused a global pandemic with over 624 million confirmed cases resulting in more than 6.5 million deaths worldwide.[9] A wide variety of methods have been developed for the detection of SARS-CoV-2 and related betacoronaviruses.[10] Although the real-time reverse transcription polymerase chain reaction (real-time RT-PCR) method is considered the gold standard for SARS-CoV-2 diagnosis, the method possesses critical drawbacks that limit the accessibility of the assay, restrict rapid treatment, and hinder important treatment-related decisions made by medical personnel under critical situations.[10] Thus, it is imperative to

Received: November 16, 2022
Accepted: January 6, 2023
Published: January 27, 2023

develop faster and more accurate diagnostic methods for this outbreak and future coronavirus pandemics, as the likelihood of encountering more virulent and rapidly spreading viruses is high[11]

Over the past few years, several different approaches for SARS-CoV-2 molecular detection have been developed to improve or substitute real-time RT-PCR. NP-based systems have gained much attention and have shown notable results in detecting SARS-CoV-2 genetic material (Table 1).[12−19]

Table 1. Recent Nanoparticle-Based Strategies for Detection of SARS-CoV-2 Genetic Material[a]

assay	target gene	LoD (copies/μL)	runtime (min)
electrochemical[12]	N, S	1	<120
electrochemical[13]	S	3.01×10^4	60
SERS[14]	E, RdRP	2.37×10^5	40
LSPR[15]	RdRP	2.26×10^4	N/A
colormetric[16]	N	10	<60
colormetric[17]	N, E	225 (N), 300 (E)	45
colormetric[18]	N	1.17×10^7	<10
fluorescence[19]	N	4	40

[a]SERS, surface-enhanced Raman spectroscopy; LSPR, localized surface plasmon resonance; N, nucleocapsid protein; S, spike protein; E, envelope protein; RdRP, RNA-dependent RNA polymerase; LoD, limit of detection.

However, the detection performances of these methods possess room for improvement as it is challenging to acquire both high sensitivity and short detection runtime for any single approach. Methods with high sensitivity often involve lengthy procedures, while faster methods generally require greater concentrations of viral genetic material for detection.

We aimed to develop an ECD system using DNA-functionalized Fe_3O_4−Au core−shell nanoparticles (CSNPs) as a nucleic acid assay platform to detect SARS-CoV-2 and additional coronaviruses that may cause future pandemics. This study presents a novel nucleic acid amplification method termed nanoparticle-based surface localized amplification (nSLAM) that uses CSNPs as multifunctional platform nanomaterial for gene amplification and accumulation. The main component of nSLAM is the CSNP, which is surface functionalized with DNA oligo primers that can amplify specific target gene sequences. The amplification procedure is identical to conventional PCR, which is well-known and easy to execute. However, the resulting products show a prominently contrasting phase as the amplicons are anchored and accumulated on the CSNP surfaces rather than in a free-standing form. Compared to previous NP-based amplification studies, the CSNPs in the nSLAM system possess great novelty as they act as dispersible nanoplatforms that directly bind to and amplify target genetic material on the NP surfaces.[12,20] The contact efficiency between the target material and DNA

Scheme 1. nSLAM Detection System Using the SARS-CoV-2 Model[a]

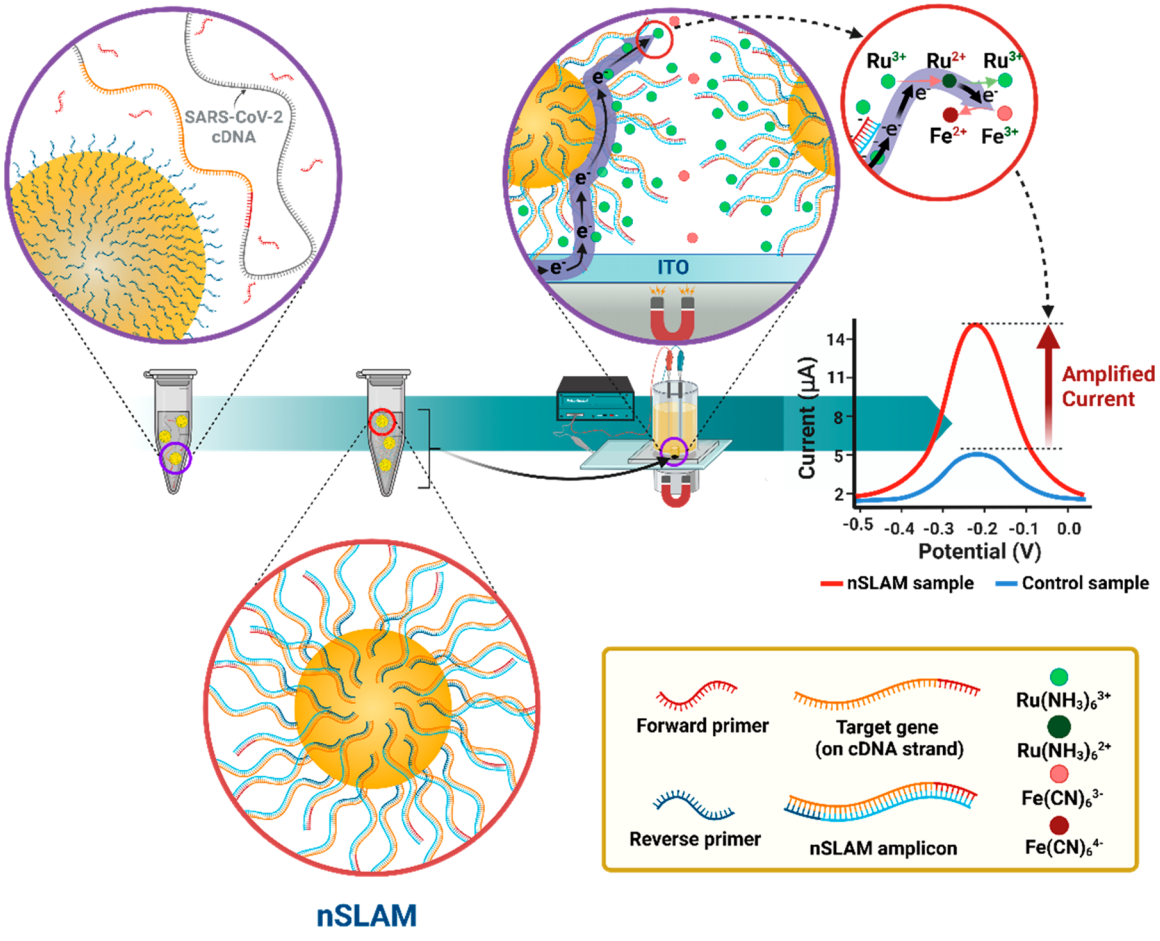

[a]Created with BioRender.

https://doi.org/10.1021/acssensors.2c02512
ACS Sens. 2023, 8, 839−847

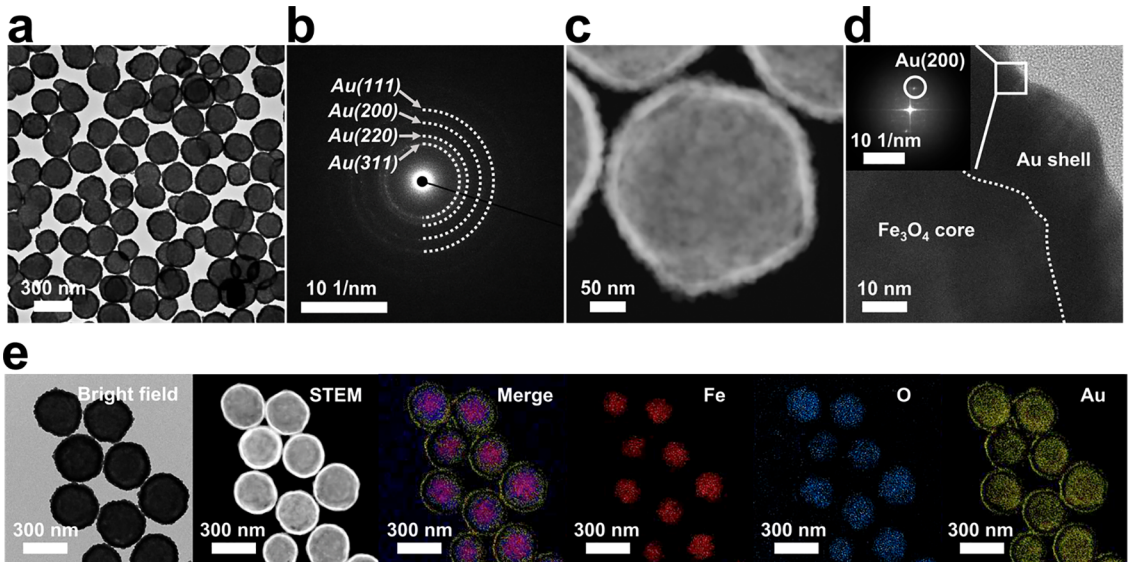

Figure 1. Morphology of CSNPs. (a) Low-magnified BFTEM images of CSNPs. (b) SAED pattern of CSNPs constructed by *fcc*-Au attributed to the (111), (200), (220), and (311) Au planes at d = 2.3, 2.0, 1.4, and 1.2 nm. (c) STEM images of CSNPs (Au shell: bright contrast, Fe_3O_4 core: dark contrast). (d) HRTEM image of CSNPs with the fast Fourier transform (FFT) pattern in the inset derived from the lattice fringe in the solid square region. (e) EDX spectroscopy/elemental mapping images of CSNPs compared with BFTEM and STEM images.

primers is significantly enhanced, which promotes amplification acceleration that is absent in conventional PCR. The amplicons remain anchored to the CSNP surfaces after amplification, which enables easy collection of the target material to electrode surfaces by applying an external magnetic field. Collection of the CSNPs results in a significant sensitivity improvement during subsequent ECD of the amplified target material, reducing amplification cycles for more rapid detection of the target.

The sensitivity of our system reached a limit of detection (LoD) of ∼1 RNA viral copy/μL with 35 cycles of amplification, demonstrating significant detection performance compared to recent NP-based SARS-CoV-2 detection systems as well as commercial SARS-CoV-2 molecular detection systems.[12−19,21,22] Further analysis regarding the reduction of amplification cycles based on the ultrasensitivity showed a minimum of 4 cycles (∼7 min runtime) to detect 1 fM of complementary DNA (cDNA), which is considerably shorter than conventional real-time RT-PCR or other detection systems.[12−19,23] Our findings indicate the significance of the nSLAM system as it is a method that enables ultrasensitive detection of SARS-CoV-2 in a rapid manner. The system is an innovative detection platform that can potentially replace conventional diagnostic methods for a more rapid, efficient, and cost-conscious response against future coronavirus-based pandemics.

RESULTS

Target Detection Using the nSLAM System. The nSLAM method promotes DNA nucleic acid amplification using multifunctional surface-functionalized magnetic CSNPs as a platform for amplicon accumulation (Scheme 1), which is the fundamental basis of our molecular detection system for pathogenic coronaviruses. Initially, CSNPs functionalized with reverse primers on particle surfaces are treated with free-standing forward primers, viral genetic material (acquired from infected human patients), and other reagents. The mixture is subjected to multiple cycles of amplification as in conventional PCR. As a result, double-stranded amplicons with target gene sequences anchor to and accumulate on the NP surfaces.

The NPs are loaded onto an electrochemical detection cell layered with an indium−tin oxide (ITO) glass sheet beneath the cell. A magnetic field is applied to the bottom of the cell to collect the NPs onto the ITO glass surface, followed by the addition of an electrocatalytic reporter pair (ERP) solution composed of ruthenium (Ru) complexes ($Ru(NH_3)_6^{3+}$) and iron (Fe) complexes ($Fe(CN)_6^{3-}$). The Ru complexes are electrostatically attracted to the negatively charged DNA backbone of the amplicons and localize near the NPs collected on the ITO glass surface. Next, an electric potential is applied to the cell using a differential pulse voltammetry (DPV) method, which has a low capacitive current, narrow voltammetric peak, and short time resolution for higher sensitivity, selectivity, and faster detection of analytes compared to other voltammetry methods.[24]

Upon application of a specific voltage, electrons travel along the ITO glass (working electrode), Au surface, and hop through the Ru complexes localized near the DNA backbone, reducing $Ru(NH_3)_6^{3+}$ to $Ru(NH_3)_6^{2+}$. The reduced Ru complex is subsequently oxidized back to $Ru(NH_3)_6^{3+}$ by a nearby Fe complex, regenerating the Ru complex to its original state.[25] The regenerated Ru complex reacts multiple times, enabling continuous oxidation and reduction of the ERP complexes. Typically, the amount of Ru complexes surrounding the DNA is limited and thus produces relatively small current signals. However, using both Ru and Fe complexes enables the continuous regeneration of Ru complexes, which has been proven to amplify current signals and increase detection sensitivity. Therefore, a significantly high redox current induced by the active movement of electrons is produced during ECD.[25]

A voltammogram with a Gaussian curve is produced with the peak positioned at the Ru complex reduction potential. The peak size depends on the amount of Ru complexes reduced, which is proportional to the number of complexes localized near the amplicons. Since complex localization is

https://doi.org/10.1021/acssensors.2c02512
ACS Sens. 2023, 8, 839−847

controlled by the quantity of negatively charged DNA backbone, nSLAM samples with double-stranded amplicons of target gene sequences produce higher current peak signals than samples with single-stranded reverse primers anchored to NP surfaces.[25] Therefore, the amplified current is an indicator of the successful amplification of the target gene through nSLAM because the absence of genetic material or the presence of nonspecific genetic material prevents the synthesis of target gene amplicons. Our system utilizes the identification of these indicators for several specific target genes to determine the existence of SARS-CoV-2 genetic material.

Characterization of CSNPs. The basis of our detection system is the CSNP that anchors reverse primers on its surface. The large surface area, strong Au−S binding interaction of the Au shell, and the exceptional magnetic property of the Fe_3O_4 core account for the high-density collection and easy extraction of amplicons using nSLAM. These advantages can be attributed to the well-defined morphology of the material acquired using elaborate procedures for particle synthesis (Supporting Information, Methods S1−S5).[26,27]

As shown in the bright-field transmission electron microscopy (BFTEM) image (Figure 1a, Supporting Information, Figure S1), CSNPs with a size of 236 ± 17 nm (184 nm sized Fe_3O_4 core, 26 nm sized Au shell) were uniformly synthesized, confirmed by the bright and dark contrast, respectively. The selected area electron diffraction (SAED) ring pattern indicated that the Au shell was deposited on the Fe_3O_4 core (Figure 1b, Supporting Information, Figure S1). The Z-contrast in the scanning transmission electron microscopy (STEM) images showed that the Au region conformally covered the surface of the Fe_3O_4 core (Figure 1c). The core−shell structure and clear interface are also supported by high-resolution transmission electron microscopy (HRTEM) and energy-dispersive X-ray (EDX) spectroscopy/elemental-mapping images of CSNPs (Figure 1d,e).

The CSNP sizes measured by transmission electron microscopy (TEM) (Figure 2a) were approximate to the intensity-based diameter of the CSNPs measured using dynamic light scattering (DLS) in an aqueous solution (Figure 2b), indicating that the NPs were well dispersed in water. Functionalization of reverse primers to the NP surface (Supporting Information, Method S6) can be identified by the increase in intensity-based diameter measurements (Figure 2b) and hydrodynamic diameter measurements (Supporting Information, Table S1). The Fe_3O_4 core of the CSNPs was synthesized using a nonclassical crystallization model developed by our group in previous studies.[27,28] Owing to this method, the CSNPs exhibited superparamagnetic properties with rapid magnetic response while maintaining an almost zero magnetic coercivity (H_c = 0.29 mT) and remanence (M_r = 0.08 emu/g), which prevented aggregation by minimizing the magnetic dipole interaction (exchange coupling) between the NPs (Figure 2c,d). Characterization of NP morphology (Supporting Information, Method S7) using various methods confirmed the physical properties of the NP and supported their use as an ideal platform for nSLAM and the electrochemical detection of genetic material.

The CSNPs used in this study were treated with primer attachment and salt-aging methods that maximized DNA loading on the NP surfaces (Supporting Information, Method S6). The average ratio of the unit NP surface area (cm^2) to the DNA footprint (nm^2) per NP unit surface area was also shown to be ∼1:1 with the larger Au−NP sizes (>200 nm diameter),

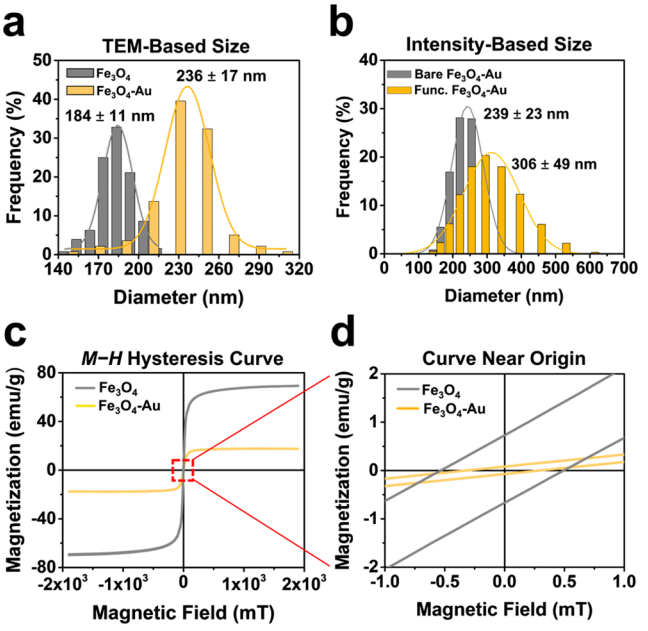

Figure 2. Size and magnetization characterization of nanoparticles. (a) Diameters of the Fe_3O_4 core and CSNPs obtained through measurements using TEM images (n > 50 nanoparticles). (b) Intensity-based sizes of bare CSNPs and primer-functionalized CSNPs measured by DLS. Mean diameters and standard deviations (s.d.) in panels a and b calculated by fitting the columns using a Gaussian function (solid lines). (c) M−H hysteresis curves of the Fe_3O_4 core and CSNPs. (d) M−H hysteresis curves near the origin.

which implied that the functionalized CSNP surfaces were densely packed with oligonucleotide primers.[5] This dense packing minimized the exposure of the Au surface, which reduced nonspecific interactions between PCR components and the NP surface that could potentially inhibit the DNA amplification process.[29]

Target Amplification with nSLAM. The amplification mechanism of nSLAM using reverse primer-functionalized CSNPs (Rp nSLAM) is an elaborate stepwise process (steps 1−8) and is illustrated in Scheme 2 with SARS-CoV-2 cDNA as the target genetic material (Supporting Information, Note S1). Multiple cycles of amplification create double-stranded amplicons with identical sizes and genetic sequences to the target gene covering the majority of the NP surface. Occasional amplicons that have both double-stranded and single-stranded sections in a single DNA complex are also formed due to the anchored long complementary single strands (Scheme 2, step 3) that create partial double-stranded DNA amplicons (Scheme 2, step 5). Conversely, nSLAM using forward primer-functionalized CSNPs (Fp nSLAM) produces uniform double-stranded amplicons of target length that accumulate on the NP surfaces.

As shown in Scheme 2 (step 8), The NPs in the Rp nSLAM sample have a greater capacity for attracting Ru complexes due to the partially double-stranded DNA amplicons that enable larger amounts of negatively charged DNA backbone to interact with the positively charged complexes electrostatically.[25] Therefore, Rp nSLAM samples produce higher ECD signals than Fp nSLAM samples using the same cDNA concentration (Supporting Information, Note S2, Figures S2 and S3, Methods S8−S10). However, the amplicon length and frequency of the partially double-stranded DNA amplicon on

https://doi.org/10.1021/acssensors.2c02512
ACS Sens. 2023, 8, 839−847

Scheme 2. Step-by-Step Process of nSLAM Using Reverse Primer Surface-Functionalized Nanoparticles (Steps 1–8)[a]

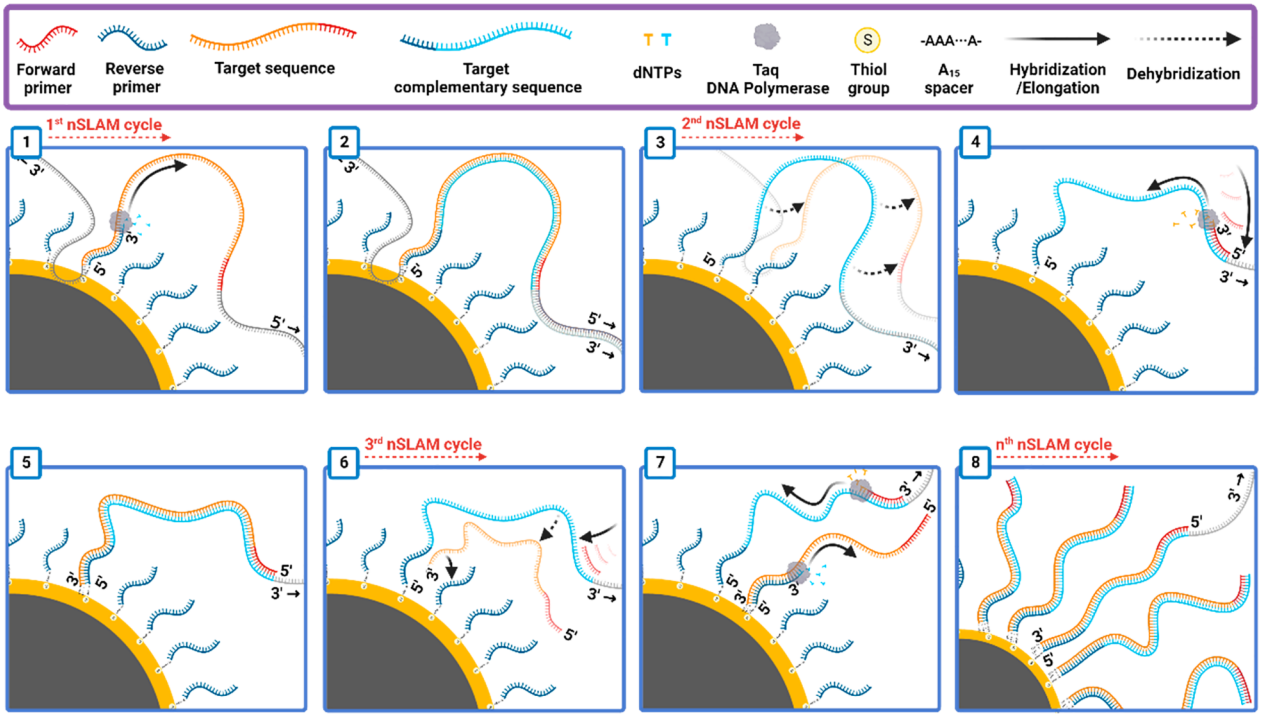

[a]SARS-CoV-2 cDNA used as the target material. Created with BioRender.

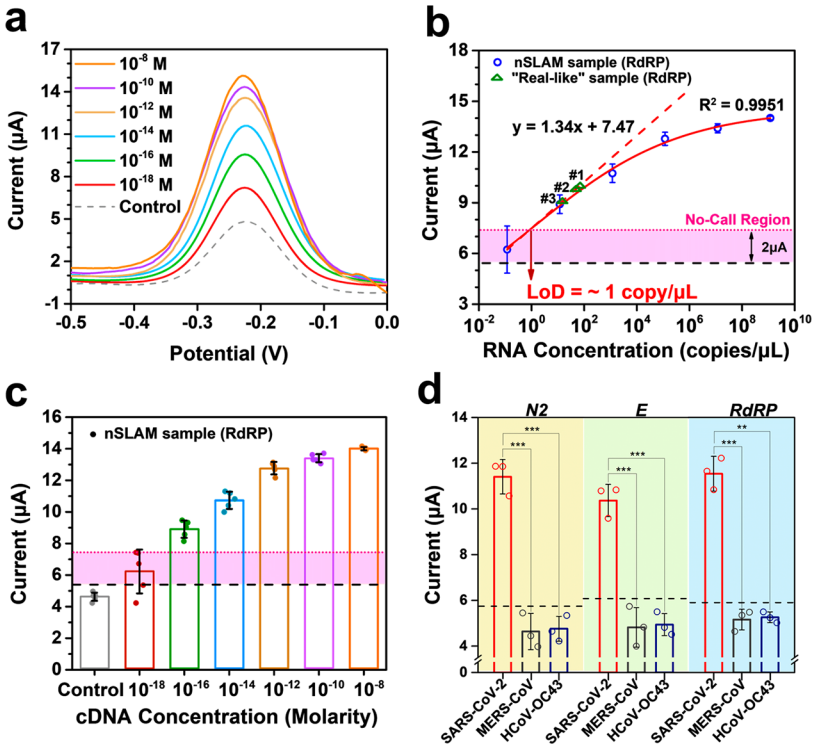

Figure 3. Sensitivity analysis of the nSLAM system. (a) Mean DPV signals of RdRP-targeted nSLAM samples (n = 5) with different cDNA concentrations. (b) ECD signals from panel a shown with an RNA concentration gradient. Mean value and s.d. of each sample expressed as individual blue circles and error bars, respectively. Logistic fitting of signals and calibration line represented as red solid curve and dashed line, respectively. Green triangles and labels represent individual "real-like" samples on the calibration line. (c) ECD signals from panel a shown with a cDNA concentration gradient. Black dashed line and shaded pink area in panels b and c represent threshold and "no-call region", respectively. (d) Cross-reactivity analysis of the nSLAM system (n = 3). Asterisks show signal contrasts between SARS-CoV-2 and nonspecific SARS-CoV-2 samples (two-sample Student's t-test). Individual ECD signals, mean values, and s.d. in panels c and d shown as dots (circles in panel d), columns, and error bars, respectively. Black dashed lines represent threshold.

https://doi.org/10.1021/acssensors.2c02512
ACS Sens. 2023, 8, 839−847

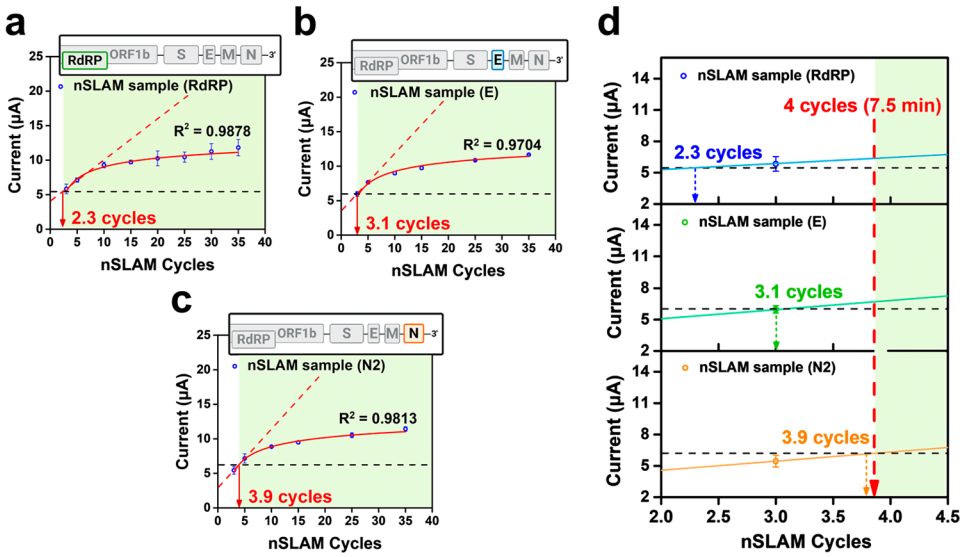

Figure 4. Runtime analysis of the nSLAM system. ECD signals of (a) RdRP-targeted nSLAM samples, (b) E-targeted nSLAM samples, and (c) N2-targeted nSLAM samples produced using different numbers of nSLAM cycles. (d) Comparison of the minimum required nSLAM cycles for detecting each target gene from panels a–c in a stacked arrangement. The mean value and s.d. of each sample (n = 3) expressed as individual circles and error bars, respectively. Logarithmic fitting of signals, calibration lines, and threshold represented as solid red curves, red dashed lines, and black dashed lines, respectively. Red dashed arrow in panel d represents the minimum nSLAM cycle number required to detect all three genes.

each CSNP are inconsistent and induce signal fluctuations between samples (Supporting Information, Figure S3). Nevertheless, the results emphasize the advantage of using reverse primer surface-functionalized NPs for nSLAM and ECD as they produce greater current signals that can enhance the detection limit of the sensor system. To verify this hypothesis, additional experiments were conducted to identify the existence of the long DNA strands anchored to NP surfaces (Scheme 2, step 3) in Rp nSLAM samples (Supporting Information, Method S11, Figures S3 and S4).

Sensitivity Analysis of the nSLAM Detection System. The ECD signal enhancement due to Rp nSLAM can potentially improve the sensitivity of a sensor as nSLAM samples produced with extremely low cDNA concentrations would generate detectable ECD signals above the threshold. Therefore, a detailed investigation of the system sensitivity regarding the LoD for the SARS-CoV-2 genetic material was conducted using a dynamic range of cDNA concentrations since the concentration of extracted genetic material can differ greatly between patients (Supporting Information, Methods S12 and S13, Figures S5 and S6).[30]

The selected target genes for amplification (Supporting Information, Figure S7) are three of the most frequently selected genes (RNA-dependent RNA polymerase (RdRP), envelope (E), and nucleocapsid (N, specifically N2 for its high sensitivity)) for SARS-CoV-2 molecular diagnosis. We implemented the World Health Organization guidelines that required positive detection of at least two different targets for positive diagnosis and selected three genes for detection, which theoretically results in a higher accuracy compared to single-target and double-target assays.[21,23,31,32] The primer sets for amplification were selected based on their sensitivity profiles and the absence of cross-reactivity with other coronaviruses tested in previous studies (Supporting Information, Figure S7, Table S2).[32−34] Of these sets, the RdRP_SARSr primer set (Charité, Germany) was selected for LoD analysis because it best represented the sensitivity of the detection system.[32]

DPV peaks of the selected cDNA concentrations in Figure 3a were converted to RNA concentrations as copies/μL based on empirical measurements of cDNA produced from reverse transcription of SARS-CoV-2 RNA (Figure 3b, Supporting Information, Table S3, Method S14). The error bars in the 1.18×10^{1}–1.18×10^{5} copies/μL range showed visible signal fluctuations (Figure 3b), which can be attributed to the previously mentioned inconsistent length and frequency of the partially double-stranded DNA amplicons that accumulate on the NP surfaces during Rp nSLAM. However, the sizable error bar at the lowest RNA concentration (1.18×10^{-1} copies/μL) indicated a lack of viral genetic material (near the Poisson limit) for nSLAM, which is expressed in Figure 3c as sporadic data points at 10^{-18} M cDNA concentration showing signals both above and below the threshold (= control signal mean + 3 × s.d. of control signal). Therefore, a "no-call region" with a range 2 μA above the threshold was established to evaluate the authenticity of the current signals and ensure the reproducibility of detectable signals. Signals and error bars within or below the "no-call region" range were considered unstable and uncertain for detection, which secured a lower limit standard for reproducible signals. The LoD was identified as the lowest concentration at which the signal exceeded the "no-call region." Based on interpolation, the calibration line intersected with the upper limit of the "no-call region" at ~1 RNA copy/μL (Figure 3b), which indicated a significantly low LoD for the RdRP target that excelled the sensitivity performance of many previously developed methods (Table 1, Supporting Information, Table S4).

Additional testing with "real-like" samples of unknown target gene RNA concentrations confirmed the validity of the calibration line as the concentrations calculated from measurements with the system were approximate to concentrations analyzed with digital PCR (Figure 3b, Supporting Information, Table S5). We also confirmed that the system eliminated nonspecific currents produced by other biological components through thorough washing, which provided a signal that was purely generated by the target gene (Supporting Information,

https://doi.org/10.1021/acssensors.2c02512
ACS Sens. 2023, 8, 839−847

Method S15). The results also verified the positive effect of the Ru−Fe ERP solution on ECD signal enhancement (Supporting Information, Figure S8).

Cross-reactivity analysis with viral strains related to SARS-CoV-2 was also conducted for all the target genes to verify whether the sensitivity results were produced with high specificity (Supporting Information, Methods S16 and 17, Note S3). The results showed that, for all target genes, nSLAM samples with SARS-CoV-2 genetic material alone produced signal values above the threshold, indicating a high level of specificity (Figure 3d, Supporting Information, Figure S9). Although the LoD of the system does not follow the criteria of other studies that analyze multiple clinical tests with at least 95% reproducibility, the significance of this value is still recognizable as a representation of the system's sensitivity expressed through the SARS-CoV-2 RdRP gene as a target.[21]

Runtime Analysis of the nSLAM Detection System. The LoD measurements emphasized the potential of the system for ultrasensitive diagnosis, which is a significant feature that can contribute to the reduction of amplification cycles needed for detection. The high sensitivity requires fewer copies of amplified gene fragments to generate ECD signals above the threshold value, which corresponds to fewer amplification cycles and shorter amplification runtimes. Therefore, we analyzed the minimum number of nSLAM cycles and amplification runtimes required for detectable levels of gene amplification (Supporting Information, Method S18). The RdRP gene was initially selected as the target for the nSLAM runtime assay. cDNA (1 fM) (~118 copies/μL RNA) (Supporting Information, Table S3), was used to match the average concentration of the clinically extracted SARS-CoV-2 genetic material (~100 copies/μL RNA) and to compare the cyclic threshold (Ct) values and detection runtime of commercial molecular diagnostic kits and NP-based detection methods with our system using similar amounts of genetic material.[12−19,22,23,35,36]

As shown in Figure 4a, the calibration line intersected with the threshold at 2.3 nSLAM cycles, which was ~1/16th the Ct value of conventional molecular diagnostic tests and significantly shorter than previous NP-based methods.[12−19,22,23] Based on these results, we analyzed E and N2 genes to test whether all target genes of our system shared similar values because the detection of all target genes must be synchronized to reduce the overall runtime.

For the N2 and E genes, a simplified nSLAM cycle range was established based on the dynamic tangent slope shift of the logarithmic function shown in Figure 4a at 3−10 nSLAM cycles, as this range appeared crucial for runtime analysis. As shown in Figures 4c,b, the lowest numbers of nSLAM cycles capable of detection in E and N2 gene-targeted nSLAM samples were identified as 3.1 and 3.9 cycles, respectively. A comparison of the three target genes (Figure 4d) near the threshold value showed that the N2 gene-targeted measurements required the highest number of nSLAM cycles at 3.9 amplification rounds, which was sufficient for detecting all targets. Thus, we concluded that at least 4 full cycles of nSLAM were required to detect all targets (Figure 4d), yielding 7.5 min for amplification leading to a major reduction in runtime compared to other molecular detection methods.[12−19,22,23]

This groundbreaking discovery emphasizes a major advantage of our system, as it compensates for a critical drawback of commercial molecular diagnostic kits and NP-based methods by significantly reducing the time spent on genetic amplification, providing faster diagnoses that facilitate rapid treatment of patients in critical conditions and assists individuals to seek immediate professional help.

DISCUSSION

The superior sensitivity, short runtime, and high specificity of our system indicate its relevance as a high-accuracy fast-response nucleic acid biosensor platform for detecting SARS-CoV-2 and potential future pandemic coronaviruses. Despite these strengths, the system is currently limited to the DNA amplification process and requires separate viral RNA extraction and reverse transcription procedures. Although there has been recent research using one-step and extraction-free methods for point-of-care diagnosis, several of them still require RNA extraction preprocessing, additional procedures before and after DNA amplification, and reaction runtimes longer than the nSLAM system.[16,37,38] These methods focus on the amplification process of nucleic acid detection, which shows significance regarding detection sensitivity and potential point-of-care treatment.[12,39] The nSLAM system presented in this study also shared this concept and aimed to enhance detection performance through the development of a novel amplification mechanism. With further research regarding the incorporation of one-step amplification and extraction-free methods, the practicality of the nSLAM system shows significant potential for improvement.

CONCLUSIONS

Using a "no-call region" as a current signal standard, the nSLAM system can detect concentrations as low as ~1 copy/μL RNA using SARS-CoV-2 genetic material, which is a significant LoD against most commercial kits and NP-based detection methods. Analysis to reduce the amplification runtime by lowering the number of nSLAM cycles showed that at least 4 cycles of nSLAM are required for the detection of the N2, E, and RdRP target genes with 1 fM cDNA (a concentration near the average extracted viral load), corresponding to a total runtime of 7.5 min with high specificity for SARS-CoV-2.

The nSLAM detection system shows great significance in the field of nucleic acid biosensors as DNA-functionalized NPs participate directly in the nucleic acid amplification process as a multifunctional platform for amplicon production and accumulation. This feature sets the system apart from other nanoparticle-based detection methods and significantly enhances the detection performance. We plan to expand the system to incorporate one-step amplification and extraction-free methods for use in point-of-care treatment. Furthermore, the integration of these methods with careful primer design can develop the system into a point-of-care multipurpose biomolecule sensor that can detect the genetic material of potentially any biomolecule of interest onsite in a short amount of time.

ASSOCIATED CONTENT

Supporting Information

The Supporting Information is available free of charge at https://pubs.acs.org/doi/10.1021/acssensors.2c02512.

BFTEM and SAED images of the Fe_3O_4 core, gel electrophoresis data of PCR amplicons, ECD signals of Rp and Fp nSLAM, sample loading and ECD scheme,

https://doi.org/10.1021/acssensors.2c02512
ACS Sens. 2023, 8, 839−847

CV voltammogram of Rp-functionalized CSNPs, primer sets and target capturing scheme, ECD signals of Ru−Fe and Ru reporter solutions including washing effects, DLS measurements of bare and reverse primer-functionalized CSNPs, primer set data used for nSLAM, conversion values of SARS-CoV-2 RNA to cDNA during RT, FDA-EUA-approved molecular detection kit data, concentrations of "real-like" samples, supporting notes, and experimental methods (PDF)

AUTHOR INFORMATION

Corresponding Authors

Young Keun Kim − *Department of Materials Science and Engineering and Brain Korea Center for Smart Materials and Devices, Korea University, Seoul 02841, Republic of Korea;* orcid.org/0000-0002-0868-4625; Email: ykim97@korea.ac.kr

Ju Hun Lee − *Department of Bionano Engineering, Hanyang University, Ansan 15588, Republic of Korea; Center for Bionano Intelligence Education and Research, Hanyang University, Ansan 15588, Republic of Korea;* orcid.org/0000-0001-7222-0510; Email: juhunlee@hanyang.ac.kr

Authors

Jeong Ook Soh − *Department of Bionano Engineering, Hanyang University, Ansan 15588, Republic of Korea; Center for Bionano Intelligence Education and Research, Hanyang University, Ansan 15588, Republic of Korea;* orcid.org/0000-0002-8108-6584

Bum Chul Park − *Department of Materials Science and Engineering and Brain Korea Center for Smart Materials and Devices, Korea University, Seoul 02841, Republic of Korea;* Present Address: Department of Chemical Engineering, University of Michigan, Ann Arbor, Michigan 48109-2136, United States

Hyeon Su Park − *Department of Materials Science and Engineering, Korea University, Seoul 02841, Republic of Korea*

Myeong Soo Kim − *Department of Materials Science and Engineering, Korea University, Seoul 02841, Republic of Korea*

Hong En Fu − *Department of Materials Science and Engineering, Korea University, Seoul 02841, Republic of Korea*

Complete contact information is available at: https://pubs.acs.org/10.1021/acssensors.2c02512

Author Contributions

⊥J.O.S., B.C.P., and H.S.P. contributed equally to this work. All authors contributed to the manuscript and have approved to the final version of the manuscript.

Notes

The authors declare no competing financial interest.

ACKNOWLEDGMENTS

This research was supported by the National Research Foundation of Korea (grant no. 2019R1A2C3006587 and 2020R1C1C1012122). This research was also supported by the Basic Science Research Program through the National Research Foundation of Korea (grant no. 2020R1A4A1016840).

REFERENCES

(1) Abi, A.; Mohammadpour, Z.; Zuo, X.; Safavid, A. Nucleic Acid-Based Electrochemical Nanobiosensors. *Biosens. Bioelectron.* **2018**, *102*, 479−489.

(2) Soleymani, L.; Fang, Z.; Sargent, E. H.; Kelley, S. O. Programming the Detection Limits of Biosensors Through Controlled Nanostructuring. *Nat. Nanotechnol.* **2009**, *4*, 844−848.

(3) Lin, M.; Pei, H.; Yang, F.; Fan, C.; Zuo, X. Applications of Gold Nanoparticles in the Detection and Identification of Infectious Disease and Biothreats. *Adv. Mater.* **2013**, *25*, 3490−3496.

(4) Ha, Y.; Kim, I. Recent Developments in Innovative Magnetic Nanoparticles-Based Immunoassays: From Improvement of Conventional Immunoassays to Diagnosis of COVID-19. *BioChip J.* **2022**, 1−365.

(5) Hill, H. D.; Millstone, J. E.; Banholzer, M. J.; Mirkin, C. A. The Role Radius of Curvature Plays in Thiolated Oligonucleotide Loading on Gold Nanoparticles. *ACS Nano* **2009**, *3*, 418−424.

(6) Mirkin, C. A.; Letsinger, R. L.; Mucic, R. C.; Storhoff, J. J. A DNA-Based Method for Rationally Assembling Nanoparticles into Macroscopic Materials. *Nature* **1996**, *382*, 607−609.

(7) Tavallaie, R.; McCarroll, J.; Le Grand, M.; Ariotti, N.; Schuhmann, W.; Bakker, E.; Tilley, R. D.; Hibbert, D. B.; Kavallaris, M.; Gooding, J. J. Nucleic Acid Hybridization on an Electrically Reconfigurable Network of Gold-Coated Magnetic Nanoparticles Enables microRNA Detection in Blood. *Nat. Nanotechnol.* **2018**, *13*, 1066−1071.

(8) Chen, D.; Wu, Y.; Hoque, S.; Tilley, R. D.; Gooding, J. J. Rapid and Ultrasensitive Electrochemical Detection of Circulating Tumor DNA by Hybridization on the Network of Gold-Coated Magnetic Nanoparticles. *Chem. Sci.* **2021**, *12*, 5196−5201.

(9) World Health Organization (WHO)*Weekly epidemiological update on COVID-19 − 26 October 2022*; World Health Organization: 2022 https://www.who.int/publications/m/item/weekly-epidemiological-update-on-covid-19---26-october-2022 (accessed October, 2022).

(10) Kevadiya, B. D.; Machhi, J.; Herskovitz, J.; Oleynikov, M. D.; Blomberg, W. R.; Bajwa, N.; Soni, D.; Das, S.; Hasan, M.; Patel, M.; Senan, A. M.; Gorantla, S.; McMillan, J.; Edagwa, B.; Eisenberg, R.; Gurumurthy, C. B.; Reid, S. P. M.; Punyadeera, C.; Chang, L.; Gendelman, H. E. Diagnostics for SARS-CoV-2 Infections. *Nat. Mater.* **2021**, *20*, 593−605.

(11) Kim, E.; Lim, E. K.; Park, G.; Park, C.; Lim, J. W.; Lee, H.; Na, W.; Yeom, M.; Kim, J.; Song, D.; Haam, S. Advanced Nanomaterials for Preparedness Against (Re-)Emerging Viral Diseases. *Adv. Mater.* **2021**, *33*, 2005927.

(12) Chaibun, T.; Puenpa, J.; Ngamdee, T.; Boonapatcharoen, N.; Athamanolap, P.; O'Mullane, A. P.; Vongpunsawad, S.; Poovorawan, Y.; Lee, S. Y.; Lertanantawong, B. Rapid Electrochemical Detection of Coronavirus SARS-CoV-2. *Nat. Commun.* **2021**, *12*, 802.

(13) Wu, C.; Chen, Z.; Li, C.; Hao, Y.; Tang, Y.; Yuan, Y.; Chai, L.; Fan, T.; Yu, J.; Ma, X.; Al-Hartomy, O. A.; Wageh, S.; Al-Sehemi, A. G.; Luo, Z.; He, Y.; Li, J.; Xie, Z.; Zhang, H. CRISPR-Cas12a-Empowered Electrochemical Biosensor for Rapid and Ultrasensitive Detection of SARS-CoV-2 Delta Variant. *Nano-Micro Lett.* **2022**, *14*, 159.

(14) Gao, Y.; Han, Y.; Wang, C.; Qiang, L.; Gao, J.; Wang, Y.; Liu, H.; Han, L.; Zhang, Y. Rapid and Sensitive Triple-Mode Detection of Causative SARS-CoV-2 Virus Specific Genes through Interaction Between Genes and Nanoparticles. *Anal. Chim. Acta* **2021**, *1154*, 338330.

(15) Qiu, G.; Gai, Z.; Tao, Y.; Schmitt, J.; Kullak-Ublick, G. A.; Wang, J. Dual-Functional Plasmonic Photothermal Biosensors for Highly Accurate Severe Acute Respiratory Syndrome Coronavirus 2 Detection. *ACS Nano* **2020**, *14*, 5268−5277.

(16) Alafeef, M.; Moitra, P.; Dighe, K.; Pan, D. RNA-Extraction-Free Nano-Amplified Colormetric Test for Point-of-Care Clinical Diagnosis of COVID-19. *Nat. Protoc.* **2021**, *16*, 3141−3162.

(17) Cao, Y.; Wu, J.; Pang, B.; Zhang, H.; Le, X. C. CRISPR/Cas12a-Mediated Gold Nanoparticle Aggregation for Colormetric Detection of SARS-CoV-2. *Chem. Commun.* **2021**, *57*, 6871.
(18) Moitra, P.; Alafeef, M.; Dighe, K.; Frieman, M. B.; Pan, D. Selective Naked-Eye Detection of SARS-CoV-2 Mediated by N Gene Targeted Antisense Oligonucleotide Capped Plasmonic Nanoparticles. *ACS Nano* **2020**, *14*, 7617−7627.
(19) Zhang, Y.; Chen, M.; Liu, C.; Chen, J.; Luo, X.; Xue, Y.; Liang, Q.; Zhou, L.; Tao, Y.; Li, M.; Wang, D.; Zhou, J.; Wang, J. Sensitive and Rapid On-Site Detection of SARS-CoV-2 Using a Gold Nanoparticle-Based High-Throughput Platform Coupled with CRISPR/Cas12-Assisted RT-LAMP. *Sens. Actuators, B* **2021**, *345*, 130411.
(20) Cheong, J.; Yu, H.; Lee, C. Y.; Lee, J. U.; Choi, H. J.; Lee, J. H.; Lee, H.; Cheon, J. Fast Detection of SARS-CoV-2 RNA via the Integration of Plasmonic Thermocycling and Fluorescence Detection in a Portable Device. *Nat. Biomed. Eng.* **2020**, *4*, 1159−1167.
(21) MacKay, M. J.; Hooker, A. C.; Afsinnekoo, E.; Salit, M.; Kelly, J.; Feldstein, J. V.; Haft, N.; Schenkel, D.; Nambi, S.; Cai, Y.; Zhang, F.; Church, G.; Dai, J.; Wang, C. L.; Levy, S.; Huber, J.; Ji, H. P.; Kriegel, A.; Wyllie, A. L.; Mason, C. E. The COVID-19 XPRIZE and the Need for Scalable, Fast, and Widespread Testing. *Nat. Biotechnol.* **2020**, *38*, 1021−1024.
(22) US Food & Drug Administration (FDA)*SARS-CoV-2 Reference Panel Comparative Data*; US Food & Drug Administration, 2020 https://www.fda.gov/medical-devices/coronavirus-covid-19-and-medical-devices/sars-cov-2-reference-panel-comparative-data (accessed December, 2021).
(23) Oh, H.; Ahn, H.; Tripathi, A. A Closer Look into FDA-EUA Approved Diagnostic Techniques of Covid-19. *ACS Infect. Dis.* **2021**, *7*, 2787−2800.
(24) Venton, B. J.; DiScenza, D. J. In *Electrochemistry for Bioanalysis*, 1st ed.; Patel, B. A.; Elsevier Science: Amsterdam, 2020; pp. 27−46.
(25) Das, J.; Ivanov, I.; Montermini, L.; Rak, J.; Sargent, E. H.; Kelley, S. O. An Electrochemical Clamp Assay for Direct, Rapid Analysis of Circulating Nucleic Acids in Serum. *Nat. Chem.* **2015**, *7*, 569−575.
(26) Kim, M. S.; Park, B. C.; Kim, Y. J.; Lee, J. H.; Koo, T. M.; Ko, M. J.; Kim, Y. K. Design of Magnetic-Plasmonic Nanoparticle Assemblies via Interface Engineering of Plasmonic Shells for Targeted Cancer Cell Imaging and Separation. *Small* **2020**, *16*, 2001103.
(27) Park, B. C.; Cho, J.; Kim, M. S.; Ko, M. J.; Pan, L.; Na, J. Y.; Kim, Y. K. Strategy to Control Magnetic Coercivity by Elucidating Crystallization Pathway-Dependent Microstructural Evolution of Magnetite Mesocrystals. *Nat. Commun.* **2020**, *11*, 298.
(28) Park, B. C.; Ko, M. J.; Kim, Y. K.; Kim, G. W.; Kim, M. S.; Koo, T. M.; Fu, H. E.; Kim, Y. K. Surface-Ligand-Induced Crystallographic Disorder-Order Transition in Oriented Attachment for the Tuneable Assembly of Mesocrystals. *Nat. Commun.* **2022**, *13*, 1144.
(29) Higashi, T.; Minegishi, H.; Nagaoka, Y.; Fukuda, T.; Echigo, A.; Usami, R.; Maekawa, T.; Hanajiri, T. Effects of Superparamagnetic Nanoparticle Clusters on the Polymerase Chain Reaction. *Appl. Sci.* **2012**, *2*, 303−314.
(30) Fajnzylber, J.; Regan, J.; Coxen, K.; Corry, H.; Wong, C.; Rosenthal, A.; Worrall, D.; Giguel, F.; Piechocka-Trocha, A.; Atyeo, C.; Fischinger, S.; Chan, A.; Flaherty, K. T.; Hall, K.; Dougan, M.; Ryan, E. T.; Gillespie, E.; Chishti, R.; Li, Y.; Jilg, N.; Hanidziar, D.; Baron, R. M.; Baden, L.; Tsibris, A. M.; Armstrong, K. A.; Kuritzkes, D. R.; Alter, G.; Walker, B. D.; Yu, X.; Li, J. Z.; The Massachusetts Consortium for Pathogen Readiness; Abayneh, B. A.; Allen, P.; Antille, D.; Balazs, A.; Bals, J.; Barbash, M.; Bartsch, Y.; Boucau, J.; Boyce, S.; Braley, J.; Branch, K.; Broderick, K.; Carney, J.; Chevalier, J.; Choudhary, M. C.; Chowdhury, N.; Cordwell, T.; Daley, G.; Davidson, S.; Desjardins, M.; Donahue, L.; Drew, D.; Einkauf, K.; Elizabeth, S.; Elliman, A.; Etemad, B.; Fallon, J.; Fedirko, L.; Finn, K.; Flannery, J.; Forde, P.; Garcia-Broncano, P.; Gettings, E.; Golan, D.; Goodman, K.; Griffin, A.; Grimmel, S.; Grinke, K.; Hartana, C. A.; Healy, M.; Heller, H.; Henault, D.; Holland, G.; Jiang, C.; Jordan, H.; Kaplonek, P.; Karlson, E. W.; Karpell, M.; Kayitesi, C.; Lam, E. C.; LaValle, V.; Lefteri, K.; Lian, X.; Lichterfeld, M.; Lingwood, D.; Liu, H.; Liu, J.; Lopez, K.; Lu, Y.; Luthern, S.; Ly, N. L.; MacGowan, M.; Magispoc, K.; Marchewka, J.; Martino, B.; McNamara, R.; Michell, A.; Millstrom, I.; Miranda, N.; Nambu, C.; Nelson, S.; Noone, M.; Novack, L.; O'Callaghan, C.; Ommerborn, C.; Osborn, M.; Pacheco, L. C.; Phan, N.; Pillai, S.; Porto, F. A.; Rassadkina, Y.; Reissis, A.; Ruzicka, F.; Seiger, K.; Selleck, K.; Sessa, L.; Sharpe, A.; Sharr, C.; Shin, S.; Singh, N.; Slaughenhaupt, S.; Sheppard, K. S.; Sun, W.; Sun, X.; Suschana, E.; Talabi, O.; Ticheli, H.; Weiss, S. T.; Wilson, V.; Zhu, A. The Massachusetts Consortium for Pathogen Readiness. SARS-CoV-2 Viral Load is Associated with Increased Disease Severity and Mortality. *Nat. Commun.* **2020**, *11*, 5493.
(31) World Health Organization (WHO)*Laboratory testing for coronavirus disease (COVID-19) in suspected human cases: interim guidance, 19 March 2020*; World Health Organization: 2020 https://apps.who.int/iris/handle/10665/331501 (accessed July, 2021).
(32) Lu, X.; Wang, L.; Sakthivel, S. K.; Whitaker, B.; Murray, J.; Kamili, S.; Lynch, B.; Malapati, L.; Burke, S. A.; Harcourt, J.; Tamin, A.; Thornburg, N. J.; Villanueva, J. M.; Lindstrom, S. US CDC Real-Time Reverse Transcription PCR Panel for Detection of Severe Acute Respiratory Syndrome Coronavirus 2. *Emerg. Infect. Dis.* **2020**, *26*, 1654−1665.
(33) Corman, V. M.; Landt, O.; Kaiser, M.; Molenkamp, R.; Meijer, A.; Chu, D. K. W.; Bleicker, T.; Brünink, S.; Schneider, J.; Schmidt, M. L.; Mulders, D. G. J. C.; Haagmans, B. L.; van der Veer, B.; van den Brink, S.; Wijsman, L.; Goderski, G.; Romette, J. L.; Ellis, J.; Zambon, M.; Peiris, M.; Goossens, H.; Reusken, C.; Koopmans, M. P. G.; Drosten, C. Detection of 2019 Novel Coronavirus (2019-nCoV) by Real-Time RT-PCR. *Eurosurveillance* **2020**, *25*, 2000045.
(34) Li, D.; Zhang, J.; Li, J. Primer Design for Quantitative Real-Time PCR for the Emerging Coronavirus SARS-CoV-2. *Theranostics* **2020**, *10*, 7150−7162.
(35) Wu, Y.; Dang, H.; Park, S. G.; Chen, L.; Choo, J. SERS-PCR Assays of SARS-CoV-2 Target Genes Using Au Nanoparticles-Internalized Au Nanodimple Substrates. *Biosens. Bioelectron.* **2022**, *197*, 113736.
(36) Jin, A.; Yan, B.; Hua, W.; Feng, D.; Xu, B.; Liang, L.; Guo, C. Clinical Characteristics of Patients Diagnosed with COVID-19 in Beijing. *Biosaf. Health* **2020**, *2*, 104−111.
(37) Li, S.; Huang, J.; Ren, L.; Jiang, W.; Wang, M.; Zhuang, L.; Zheng, Q.; Yang, R.; Zeng, Y.; Luu, L. D. W.; Wang, Y.; Tai, J. A One-Step, One-Pot CRISPR Nucleic Acid Detection Platform (CRISPR-Top): Application for the Diagnosis of COVID-19. *Talanta* **2021**, *233*, 122591.
(38) Smyrlaki, I.; Ekman, M.; Lentini, A.; de Sousa, N. R.; Papanicolaou, N.; Vondracek, M.; Aarum, J.; Safari, H.; Muradrasoli, S.; Rothfuchs, A. G.; Albert, J.; Högberg, B.; Reinius, B. Massive and Rapid COVID-19 Testing is Feasible by Extraction-Free SARS-CoV-2 RT-PCR. *Nat. Commun.* **2020**, *11*, 4812.
(39) Afzal, A. Molecular Diagnostic Technologies for COVID-19: Limitations and Challenges. *J. Adv. Res.* **2020**, *26*, 149−159.

https://doi.org/10.1021/acssensors.2c02512
ACS Sens. 2023, 8, 839−847